Disturbance Rejection Analysis and FPGA based Implementation of a Second Order Sliding Mode Controller fed Induction Motor Drive

A. V. Ravi Teja, *Member, IEEE*, Chandan Chakraborty, *Fellow, IEEE* and Bikash Pal, *Fellow, IEEE*

***Abstract*—This paper presents a unified approach to deal with sliding mode controllers used for induction motor drives. The study digs deep to identify matched and unmatched disturbances and derive conditions to satisfactorily reject the same. The investigation reveals fundamental limitations of hysteresis (first order sliding mode) controllers those can be overcome by higher order controllers. Second order sliding mode controllers are investigated to achieve disturbance rejection and chattering free performance. It is shown that the drive with second order sliding mode controllers maintains constant switching frequency and decoupling between torque and flux simultaneously in the face of sudden speed, load, or parameter variations. Also, it is shown that the dynamic performance can be drastically improved at higher sampling frequencies keeping the switching frequency constant. Extensive simulations are carried out in Matlab/Simulink. Implementation of such a drive becomes feasible with low cost FPGAs due to their inherent parallel processing capability. A vector controlled induction motor drive is developed and the controller is implemented using FPGA to corroborate the simulation results through experimentations.**

***Index Terms*—Induction motor drives, PWM operation, hysteresis current controlled converter, vector control, higher order sliding mode control, FPGA.**

I. Introduction

INDIRECT vector control of squirrel cage induction motor drives is a very popular control strategy providing high dynamic performance. Sliding mode control (SMC) is a well established nonlinear control strategy for enhancing performance robustness and offering effective disturbance rejection [1]. In vector controlled induction motor drives, SMC is applied in two ways, one as an observer for estimating machine quantities [2]–[11] and the other as a controller for error convergence [12]–[17]. Since observers are model-based which are parameter dependent, sliding mode controllers when used in observers cannot offer as much disturbance rejection as they can when used as controllers. A sliding mode controller can be of first order [12], [13] (a simple signum function otherwise called hysteresis controller) or of higher order [17]–[20].

In vector controlled drives, hysteresis current controller fed PWM technique is widely used to generate the switching pulses for the inverter. The known advantages of hysteresis PWM technique are fast response, ease of implementation, and inherent over-current protection [12], [13]. However, the dynamics and disturbance rejection ability of such a drive need to be clearly established. This paper is an attempt to apply sliding mode concepts to vector controlled induction motor drive and understand the dynamics and disturbance rejection properties of the system.

The major problem of hysteresis PWM is variable switching frequency resulting in distortion of line currents. Researchers tackled this disadvantage and achieved constant switching frequency in two ways, one by modifying the hysteresis band at every load and operating point [13] and the other is by using PI controllers along with parameter dependent feed forward terms [21]. As seen, these methods are operating point or machine parameter dependent, which vary normally during the operation of the drive. In PI controller based methods, integral sliding mode control is employed in [21]–[23] to remove the parameter dependency of the feed forward terms but these methods suffer from chattering and other performance related issues.

In literature, some authors have reported the use of higher order sliding mode controllers for induction machine [2], [9], [11], [14], [15], [17]. While most of these works used SMC as an observer [2], [9], [11], the authors in [14], [15], [17] used an SMC as a controller. In this paper, a vector controlled IM drive is analyzed from the perspective of sliding mode control. A unified approach is presented. In addition, the following contributions are highlighted.

- The disturbance rejection conditions are derived in terms of closed-form expressions. Influence of matched and unmatched disturbances on the system is studied.
- It is demonstrated that the drive with second order sliding mode controllers maintains constant switching frequency. Effect of increasing the sampling frequency on the performance of the drive is also investigated.
- The propositions are implemented and verified experimentally using a low cost FPGA based hardware setup developed in the laboratory. Implementation aspects in FPGA are also presented.

The paper is presented in nine sections. Section-I provides a brief introduction of the work, whereas a review of the sliding mode concepts is presented in Section-II. These concepts are applied to a hysteresis PWM fed indirect vector controlled induction motor drive in Section-III and its dynamics and its disturbance rejection properties are studied in Section-IV. The use of second order sliding modes, their implementation, dynamics, and disturbance rejection properties are discussed in Section-V. Section-VII reports the simulation results using MATLAB/SIMULINK. A low cost FPGA based experimental setup is developed in the laboratory (Section-VIII) and the

experimental results are presented in Section-IX. Section-X concludes the work.

II. Review of Sliding Mode Control Theory

A. Introduction [1]

The first order sliding mode control (SMC) input (u) in a single input single output system $\dot{x} = u + d$ to reach sliding surface 's' is given as

$$u = -k\text{sign}(s \pm \epsilon) \tag{1}$$

where $k > |d|$, 'd' is the disturbance in the system and ϵ is the size of the hysteresis band.
The following points can be noted from first order SMC:

- The disturbance must be matched with the input in order to get rejected.
- The actual quantities of all the states required in the sliding surface s are sensed and fed to controller for satisfactory operation of the SMC.
- The kind of SMC in (1) can be applied only to systems with relative degree one.

Further SMC concepts like *equivalent control method* for obtaining the dynamics of the system in sliding mode, *hyperplane vector transformation* for applying SMC in multi-input case, and *cascaded control* for using SMC to reject unmatched disturbances are discussed briefly in the following subsections.

B. Equivalent Control Method

Due to the switching nature of the control input, it is difficult to study a system under SMC analytically. So, in order to study about the stability and dynamic response of systems containing sliding modes, Utkin [1] developed equivalent control method where we can obtain the equivalent continuous-time control input applied to the system.
Let us assume a general system as:

$$\dot{x} = f(x,t) + Bu \tag{2}$$

where $x_{m\times 1}$, $f(x,t)_{m\times 1}$, $B_{m\times n}$, $u_{n\times 1}$, $m, n \in \Re$.
For this system with a designed sliding surface $s = 0$, the expression for equivalent control input, u_{eq} is given as

$$u_{eq} = -[GB]^{-1}Gf(x,t) \tag{3}$$

where $G(x)_{n\times m}$ denotes the gradient of the scalar surface i.e., the jacobian matrix. Substituting (3) in (2), we get

$$\dot{x} = [I - B[GB]^{-1}G]f(x,t) \tag{4}$$

where I is the identity matrix of appropriate order. Therefore, the dynamics and stability of the system in sliding mode can be studied using the continuous equivalent system given in (4).

C. Cascaded Control

In order to reject unmatched disturbances, the concept of cascaded control is proposed in [24]. To understand this, let us assume a system to be of the form

$$\begin{aligned}\dot{x}_1 &= f_1(t,x_1) + g_1(t,x_1)x_2 + dd_1(t,x)\\ \dot{x}_2 &= f_2(t,x_1,x_2) + g_2(t,x_1,x_2)u + dd_2(t,x)\end{aligned} \tag{5}$$

where $dd_1(t,x)$ and $dd_2(t,x)$ are the disturbances to be rejected. If the sliding surface $s = x_1 - x_1^* = 0$ (x_1^* is the reference value), then the relative degree of the system is two. It can be observed here that $dd_1(t,x)$ is an unmatched disturbance since it does not appear along with the input u whereas $dd_2(t,x)$ is a matched disturbance which can be rejected. In order to reject both $dd_1(t,x)$ and $dd_2(t,x)$, the concept of virtual control is proposed in [24]. According to this, x_2 is defined as a virtual control input for which $dd_1(t,x)$ becomes a matched disturbance and so it can be rejected using the sliding surface $s = x_1 - x_1^* = 0$. Then, actual x_2 is forced to match this virtual control input using another sliding surface, $x_2 - x_2^* = 0$ (x_2^* is the virtual control input) using input u defined in (5) and this can reject matched disturbance $dd_2(t,x)$. Hence, both matched and unmatched disturbances can be rejected with this technique.

III. Hysteresis PWM and Vector Control

The concepts of SMC briefly explained in the previous section are now applied to a hysteresis PWM fed vector controlled induction motor drive.

A. Sliding Surfaces in Vector Control

In a vector controlled induction motor drive, current controller errors are chosen as sliding surfaces since they are directly related with the inputs as:

$$\begin{bmatrix}\dot{i}_{sd}\\ \dot{i}_{sq}\end{bmatrix} = \begin{bmatrix}a_1 i_{sd} + \omega_e i_{sq} + a_2\psi_{rd} + a_3\omega_r\psi_{rq}\\ a_1 i_{sq} - \omega_e i_{sd} + a_2\psi_{rq} - a_3\omega_r\psi_{rd}\end{bmatrix} + \frac{1}{\sigma L_s}\begin{bmatrix}v_{sd}\\ v_{sq}\end{bmatrix} \tag{6}$$

Therefore, the sliding hyperplane is given by

$$s = \begin{bmatrix}s_1\\ s_2\end{bmatrix} = \begin{bmatrix}i_{sd} - i_{sd}^*\\ i_{sq} - i_{sq}^*\end{bmatrix} \tag{7}$$

B. Concept of Cascaded Control in Vector Control

The induction machine is modeled in synchronously rotating rotor flux reference frame [25] taking stator current and rotor flux as state variables. The state-space model is given by

$$\begin{bmatrix}\dot{i}_{sd}\\ \dot{i}_{sq}\\ \dot{\psi}_{rd}\\ \dot{\psi}_{rq}\end{bmatrix} = \begin{bmatrix}a_1 & \omega_e & a_2 & a_3\omega_r\\ -\omega_e & a_1 & -a_3\omega_r & a_2\\ \dfrac{L_m}{\tau_r} & 0 & -\dfrac{1}{\tau_r} & \omega_{sl}\\ 0 & \dfrac{L_m}{\tau_r} & -\omega_{sl} & -\dfrac{1}{\tau_r}\end{bmatrix}\begin{bmatrix}i_{sd}\\ i_{sq}\\ \psi_{rd}\\ \psi_{rq}\end{bmatrix} + \frac{1}{\sigma L_s}\begin{bmatrix}v_{sd}\\ v_{sq}\\ 0\\ 0\end{bmatrix} \tag{8}$$

where

$$a_1 = -\frac{1}{\sigma L_s}\left[R_s + \frac{L_m^2}{L_r\tau_r}\right], a_2 = \frac{1}{\sigma L_s}\frac{L_m}{L_r\tau_r}, a_3 = \frac{1}{\sigma L_s}\frac{L_m}{L_r} \tag{9}$$

and

$$\omega_{sl} = \omega_e - \omega_r = \frac{1}{\tau_r}\frac{i_{sq}}{i_{sd}^*} \tag{10}$$

The mechanical equation of the machine with electromagnetic torque (T_e) and load torque (T_L) is given by

$$(T_e - T_L)\frac{P}{2} = J\dot{\omega}_r + \mathrm{B}\omega_r \tag{11}$$

where

$$T_e = \frac{3}{2}\frac{P}{2}\frac{L_m}{L_r}(\psi_{rd}i_{sq} - \psi_{rq}i_{sd}) \tag{12}$$

The core of vector control is the flux control. In rotor flux oriented reference frame, rotor flux is maintained constant ($\psi_{rd} = \psi^*_{rd} = L_m i^*_{sd}$) by keeping i_{sd} constant at i^*_{sd}. Therefore, one sliding surface is selected as $s_1 = i_{sd} - i^*_{sd}$. This dynamics can be understood by considering the expression for $\dot{i}_{sd}$ from (8) as follows.

$$\dot{i}_{sd} = a_1 i_{sd} + \omega_e i_{sq} + a_2\psi_{rd} + a_3\omega_r\psi_{rq} + \frac{1}{\sigma L_s}v_{sd} \tag{13}$$

Eqn. (13) can be compared with standard first order system with matched disturbance, $\dot{x} = u + d$ where $u = \frac{1}{\sigma L_s}v_{sd}$ and $d = a_1 i_{sd} + \omega_e i_{sq} + a_2\psi_{rd} + a_3\omega_r\psi_{rq}$. Therefore, input u can be applied such that disturbance d is rejected. Since the actual machine is in stationary reference frame, the kind of input defined in (1) cannot be applied directly. We have to go for hyperplane vector transformation into stationary reference frame which will be discussed later.

Now for the drive system, the speed/torque control has to be exercised. For torque control, the sliding surface is chosen as $s_2 = i_{sq} - i^*_{sq}$, the torque current error. For this sliding surface, the analysis is similar if "i_{sq}" is considered instead of "i_{sd}". For speed control, consider the following equations obtained from (8),(11), and (12) for a vector controlled drive under rotor flux orientation ($\psi_{rd} = \psi^*_{rd}$ and $\psi_{rq} = 0$).

$$\begin{aligned}\dot{\omega}_r &= \left[\frac{3}{2}\frac{P}{2}\frac{L_m}{L_r}\psi^*_{rd}i_{sq} - T_L\right]\frac{P}{2J} - \frac{\mathrm{B}}{J}\omega_r \\ \dot{i}_{sq} &= -\omega_e i_{sd} + a_1 i_{sq} - a_3\omega_r\psi_{rd} + \frac{1}{\sigma L_s}v_{sq}\end{aligned} \tag{14}$$

Eqn. (14) is of the same form as (5) where $x_1 = \omega_r$, $u = v_{sq}$, and the virtual control input $x_2 = i_{sq}$. Therefore, unmatched disturbances (not along the input v_{sq}) like load torque variation as well as matched disturbances can be rejected completely with this approach of *cascaded control*. From this, the condition on the input voltage for satisfactory disturbance rejection is derived as presented in Section IV.

C. Equivalent Control in Vector Control

Since the system is now defined from SMC principles, we can now relate the system with the concept of *equivalent control* to determine the dynamics of the system in the sliding mode. Using (6) and (3), the equivalent control input is given as:

$$\begin{aligned}u_{eq} &= -[GB]^{-1}Gf(x,t) \\ &= -[GB]^{-1}\begin{bmatrix}a_1 i_{sd} + \omega_e i_{sq} + a_2\psi_{rd} + a_3\omega_r\psi_{rq} \\ a_1 i_{sq} - \omega_e i_{sd} + a_2\psi_{rq} - a_3\omega_r\psi_{rd}\end{bmatrix}\end{aligned} \tag{15}$$

and the dynamics of the system in sliding mode is given by (4) as

$$\dot{x} = \begin{bmatrix}\dot{i}_{sd} \\ \dot{i}_{sq}\end{bmatrix} = [I - B[GB]^{-1}G]f(x,t) = \begin{bmatrix}0 \\ 0\end{bmatrix} \tag{16}$$

This means that the system (6) in sliding mode behaves as if the first derivative of the system states i_{sd} and i_{sq} are zero. It is well known that a system under SMC behaves like a reduced order system. The same applies here also. Since $\dot{i}_{sd}$ and $\dot{i}_{sq}$ became zero, the system order gets reduced by 2. Therefore, by the application of sliding modes, the fifth order induction machine behaves like a third order system.

IV. Disturbance Rejection

One of the major advantages of SMC is disturbance rejection. This section deals with the effect of disturbances like load torque variation, parameter variation, etc. on the system.

A. Rejection to matched disturbances

SMC naturally rejects the matched disturbances if the control input is sufficiently large. The matched disturbances for the system (6) are given as

$$\begin{bmatrix}d_1 \\ d_2\end{bmatrix} = \begin{bmatrix}a_1 i_{sd} + \omega_e i_{sq} + a_2\psi_{rd} + a_3\omega_r\psi_{rq} \\ a_1 i_{sq} - \omega_e i_{sd} + a_2\psi_{rq} - a_3\omega_r\psi_{rd}\end{bmatrix} \tag{17}$$

To reject these disturbances satisfactorily, the control inputs in d-q frame must satisfy the following condition

$$\begin{bmatrix}v_{sd} \\ v_{sq}\end{bmatrix} > \begin{bmatrix}|\sigma L_s(a_1 i_{sd} + \omega_e i_{sq} + a_2\psi_{rd} + a_3\omega_r\psi_{rq})| \\ |\sigma L_s(a_1 i_{sq} - \omega_e i_{sd} + a_2\psi_{rq} - a_3\omega_r\psi_{rd})|\end{bmatrix} \tag{18}$$

Squaring and adding v_{sd} and v_{sq}, we get

$$v_{sd}^2 + v_{sq}^2 > (\sigma L_s)^2(d_1^2 + d_2^2) \tag{19}$$

Using Clarke's transformation and equating $v_{sa}+v_{sb}+v_{sc} = 0$, we get

$$v_{sd}^2 + v_{sq}^2 = (v_{sa})^2 + \left(\frac{v_{sb}}{\sqrt{3}} - \frac{v_{sc}}{\sqrt{3}}\right)^2 \geq v_{sa}^2 = k_1^2 \tag{20}$$

In a vector controlled drive fed from an inverter, k_1 is the pole voltage which is equal to $V_{dc}/2$ (where V_{dc} is the dc bus voltage). Therefore, the approximate condition on dc bus voltage for satisfactory rejection of d_1 and d_2 is given as

$$V_{dc} \geq 2\sigma L_s\sqrt{(d_1^2 + d_2^2)} \tag{21}$$

B. Rejection to unmatched disturbances

SMC cannot directly reject unmatched disturbances but as shown in previous section, using cascaded control strategy, these disturbances can be rejected by the use of virtual control. For understanding this, the first part of (14) is considered again by replacing i_{sq} with u_{vir} (indicating virtual control input) as

$$\dot{\omega}_r = \left[\frac{3}{2}\frac{P}{2}\frac{L_m}{L_r}\psi^*_{rd}u_{vir} - T_L\right]\frac{P}{2J} - \frac{\mathrm{B}}{J}\omega_r \tag{22}$$

After the introduction of virtual control, the disturbances which were unmatched with the actual input became matched with the virtual control input. The disturbance that can now be rejected is:

$$d_3 = -T_L\frac{P}{2J} - \frac{\mathrm{B}}{J}\omega_r \tag{23}$$

and the condition on the virtual control input for satisfactory operation rejecting disturbance d_3 is given as

$$u_{vir} > \left|\left(-T_L\frac{P}{2J} - \frac{\mathrm{B}}{J}\omega_r\right)\frac{4L_r}{3PL_m\psi^*_{rd}}\right| \tag{24}$$

This u_{vir} is considered as the reference q-axis current i^*_{sq} to form the second sliding surface s_2 in the hyperplane s. By doing so, both the disturbances d_2 and d_3 are simultaneously rejected and disturbance d_1 is anyway rejected using first sliding surface s_1.

C. Disturbances that cannot be rejected

It is important to note that there are disturbances that cannot be rejected in a hysteresis PWM fed vector controlled induction motor drive. It comes from the fact that the feedback currents i_{sd} and i_{sq} in the sliding hyperplane s (7) are not directly available for sensing. If the actual values of i_{sd} and i_{sq} are sensed, the entire system could have been free from all disturbances but unfortunately the machine is in a-b-c reference frame and currents in this reference frame can only be sensed. The relation between a-b-c and d-q reference frame currents is given as

$$\begin{bmatrix} i_{sd} \\ i_{sq} \end{bmatrix} = \begin{bmatrix} \frac{2}{3}\cos\theta_e & -\frac{\cos\theta_e}{3} + \frac{\sin\theta_e}{\sqrt{3}} & -\frac{\cos\theta_e}{3} - \frac{\sin\theta_e}{\sqrt{3}} \\ -\frac{2}{3}\sin\theta_e & \frac{\sin\theta_e}{3} + \frac{\cos\theta_e}{\sqrt{3}} & \frac{\sin\theta_e}{3} - \frac{\cos\theta_e}{\sqrt{3}} \end{bmatrix} \begin{bmatrix} i_{sa} \\ i_{sb} \\ i_{sc} \end{bmatrix} \tag{25}$$

As shown in (25), the d-q frame currents are obtained from the sensed a-b-c frame currents using the position of the rotor flux vector θ_e. Therefore, the computation of i_{sd} and i_{sq} is sensitive to the parameters involved in the computation of θ_e. In indirect vector control, θ_e is obtained as

$$\theta_e = \int \omega_e dt = \int (\omega_r + \omega_{sl})dt \tag{26}$$

where ω_{sl} is given by (10). Assuming that the speed signal ω_r is sensed directly, the influencing parameter is the rotor time constant τ_r in the slip equation. Any mismatch in the parameter τ_r results in wrong estimation of i_{sd} and i_{sq} which in turn results in reaching the wrong sliding surfaces. Thus, the whole system becomes sensitive to τ_r variation and hence these disturbances cannot be rejected by SMC. Similarly, if the rotor speed is estimated, then the system becomes sensitive to all the parameters present in the rotor speed estimation algorithm.

V. Higher Order Sliding Mode Control

The problem with hysteresis PWM (which is basically a first order SMC) are chattering and operation at variable switching frequency. To overcome this without losing the disturbance rejection properties, higher order sliding mode control [18]–[20], [26] is recommended. According to higher order sliding mode control theory [20], for the system (6) with relative degree one, the order of the sliding modes must be at least two to eliminate chattering. Also, the system complexity increases with increase in sliding mode order. Therefore, a second order sliding mode is used.

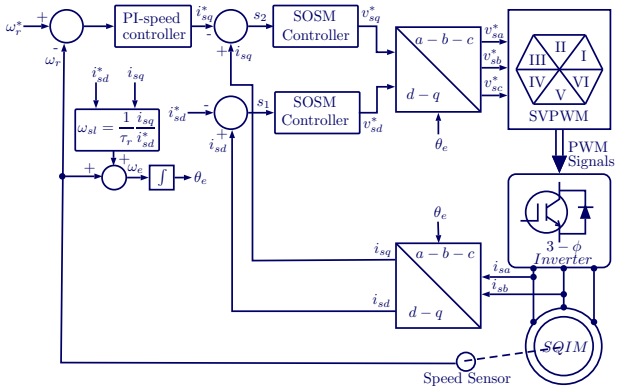

Fig. 1. Indirect vector controlled IM drive with second order SMC current controllers.

A. Second Order Sliding Mode Control

There are several second order sliding mode controllers proposed in literature [18]–[20], [26]. Of these, the one in [18], [19] can be easily implemented and is given as

$$\dot{u} = -r_1\mathrm{sign}(s) - r_2\mathrm{sign}(\dot{s}) \tag{27}$$

where $r_1 > r_2 > 0$. As shown in (27), the sign terms (chattering causing terms) are now present in the derivative of the input u. Therefore, by proper selection of r_1 and r_2, chattering can be removed from actual control input u obtained by integrating $\dot{u}$. The block diagram of the vector controlled drive [25] with second order sliding mode current controllers is shown in Fig. 1. As seen, the current controllers are replaced with second order sliding mode controllers to reach sliding surfaces $s_1 = i_{sd} - i^*_{sd}$ and $s_2 = i_{sq} - i^*_{sq}$. The speed controller is a PI controller. From Fig. 1, it can be observed that since the outputs of a second order SMC are continuous, space vector PWM modulation is employed to maintain constant switching frequency and to achieve enhanced dc bus utilization of the inverter. The outputs of the second order SMC are given as

$$\begin{bmatrix} v^*_{sd} \\ v^*_{sq} \end{bmatrix} = \begin{bmatrix} \int\{-r_{11}\mathrm{sign}(s_1) - r_{21}\mathrm{sign}(\dot{s}_1)\}dt \\ \int\{-r_{12}\mathrm{sign}(s_2) - r_{22}\mathrm{sign}(\dot{s}_2)\}dt \end{bmatrix} \tag{28}$$

where s_1 and s_2 are defined in (7). The tuning procedure of the sliding mode gains is given in [27].

B. Disturbance Rejection using second order SMC

All the concepts of sliding mode control discussed in Sections-II, III, and IV hold true even for second order sliding modes with the only difference that along with the disturbance d being bounded, the derivative of the disturbance i.e., $\dot{d}$ also must be bounded since the output of the second order sliding

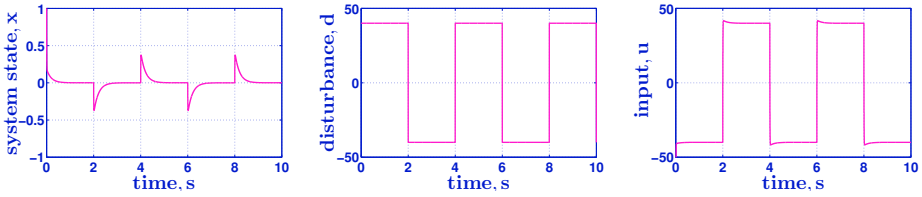

(a) (b) (c)

Fig. 2. Simulation Result with PI control. (a) System state 'x'. (b) Disturbance 'd'. (c) input 'u'.

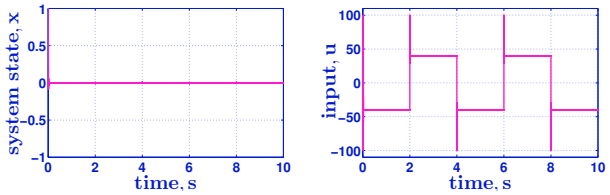

(a) (b)

Fig. 3. Simulation Result with SOSM control. (a) System state 'x'. (b) input 'u'.

mode control is $\dot{u}$ instead of u. Therefore, the condition on the derivative of the disturbance is given as

$$\frac{1}{\sigma L_s}\begin{bmatrix}\dot{v}_{sd}\\ \dot{v}_{sq}\end{bmatrix} > \begin{bmatrix}|\dot{d}_1|\\ |\dot{d}_2|\end{bmatrix} \tag{29}$$

where d_1 and d_2 are defined in (17).

C. Discretization of the Controller

The controller given in (27) has to be discretized for digital implementation in FPGA. Discretization is done using Euler's method which approximates the continuous domain terms and hence the twisting control also is expected to approximate the performance of its corresponding continuous domain. It has been proved in [18] that the real sliding due to discretization will converge the sliding surface within $|s| < k_1 T_s^2$ and $|ds/dt| < k_2 T_s$ where $k_1, k_2 > 0$ and T_s is the sampling time used for discretization. This error will be very small if the sampling time, T_s used is small. Therefore, the value of input u at k^{th} instant is given as

$$u_k = u_{k-1} + T_s\{-r_1 \text{sign}(s_k) - r_2 \text{sign}(s_k - s_{k-1})\} \tag{30}$$

where s_k is the sliding surface at k^{th} sampling instant and T_s is the sampling time of the system. As seen from (30), for getting the information about sign of the derivative of s, we need not compute the actual derivative. The sign of $s_k - s_{k-1}$ is the same as the sign of $\dot{s}$ and hence the problems related to practical implementation of derivative operation can be avoided.

VI. Comparison With a PI Controller

PI controllers are traditionally used in the speed and current loops of vector control in order to maintain constant switching frequency of the inverter. While PI controllers can also reject disturbances eventually, they cannot make the closed loop system immune to disturbances i.e., they cannot provide reduced order behavior to the system like a sliding mode controller. This can be better understood by considering again the simple system, $\dot{x} = u + d$ discussed in Section-II applied with a disturbance as shown in Fig. 2b. Here, the error $e = 0 - x$ is processed through a PI controller (k_P =200 and k_I =1000) to get input u and the results are reported in Fig. 2. As shown in Fig. 2a, the system state is affected for every change in the disturbance d (Fig. 2b) but it eventually reverts back to zero due to the PI action. Thus, we can say that the system is not completely immune to disturbances but can reject them eventually. This is the disadvantage of using PI as current controllers because in a vector controlled drive, it is required that the d- and q-axis current errors remain zero irrespective of disturbances.

Let us now see the effect of using a SOSM controller (27) in place of a PI controller. The result is shown in Fig. 3 (for $r_1 = 2 \times 10^5$ and $r_2 = 4 \times 10^4$) when the same disturbance (Fig. 2b) is applied on the system. It can be observed from Fig. 3b that the input has fast dynamics and is continuous. The system state x is immune to disturbances (x remains zero even with sudden changes in disturbances) as shown in Fig. 3a thus making an SOSM controller more suitable for use as current controllers in a vector controlled drive. Also, it can be observed that the computational burden of an SOSM controller (27) is almost the same as that of a PI controller requiring one integration, two gain multiplications, and two add/subtract operations. In addition, the SOSM controller requires two sign operations consuming negligible resources of the processor.

In a vector controlled drive, unlike the current controllers, the speed response depends on the inertia of the machine. Thus, an SOSM controller if used in the speed loop of a vector controlled IM drive may always give an i_{sq}^* which is beyond the permissible limits or in other words the output of the speed loop gets saturated at the maximum values for most of the time depending on the sudden changes in reference speed and mechanical time constant of the machine. The sliding mode controller action is lost whenever it hits saturation. To avoid this, it is better to use a slow acting PI controller in the outer speed loop instead of a fast acting SOSM controller. Since a PI controller can also reject disturbances, the speed loop PI can reject disturbance d_3 (23) but as discussed earlier, the speed loop will not be immune to disturbances. This is also good from mechanical stress point of view of the machine

shaft. Thus, a PI controller in the speed-loop is sufficient to have desired performance for the overall system. The final conclusion is to employ an SOSM controller in the inner current loops and a PI controller in the outer speed loop of the vector controlled induction motor drive as in Fig. 1.

VII. Simulation Results

The disadvantages of using hysteresis current controllers are well reported in literature [21] and hence these results are not repeated. The simulation results (using MATLAB/SIMULINK) presented in this section mainly highlight to show the disturbance rejection and chattering free nature of second order SMC fed drive (Fig. 1) for sudden speed, load, and parameter variations. While load varation is an unmatched disturbance, stator resitance variation is a matched disturbance. Stator resistance parameter variation is considered in this study since it is not involved in θ_e calculation and hence can be rejected by sliding mode control. Also, stator resistance can be easily varied in hardware (by connecting external resistances in series with the stator terminals) to produce the corresponding experimental result. The machine parameters are given in Table I.

A. IM drive with second order SMC Current Controller

The performance of the drive with second order SMC current controllers (Fig. 1) is shown in Fig. 4. Speed, load and stator resistance variations are considered one after the other in a single result for conciseness. The speed PI and second order SMC current controller values are chosen to satisfy (18), (29) and their values are given in Table II. The sampling frequency of the system is kept at 6.103 kHz. The system is simulated for a step change in speed of 20 rad/s applied at 2s from start (Fig. 4a), followed by a load change to 0.5 pu at 5.4s (Fig. 4c), and then the stator resistance parameter is suddenly varied to triple its value at 7.7s and again returned back to its original value at 9s (Fig. 4f). The speed response is shown in Fig. 4a where the reference speed matches with actual. A sudden dip in speed occurs on loading and the actual speed restores back to reference speed. There is no chattering observed in i_{sd} and i_{sq} waveforms as seen in Figs. 4b and 4c. A closer view showing the dynamic response of torque component of current is given in Fig. 4d. The i_{sq} dynamics take about 10 ms to reach i^*_{sq} as shown but this change has negligible effect on the d-axis current (Figs. 4b) which is a clean waveform with no chattering. This is due to continuous nature of the second order SMC output. Along with this, since the nature of sliding mode control is to remain immune to disturbances, decoupling is maintained inherently between i_{sd} and i_{sq}. Since the flux component of current i_{sd} remained immune to speed, load, or stator resistance variation disturbances as shown in Fig. 4b, flux orientation is well maintained irrespective of disturbances. From Fig. 4c, it can be seen that the torque component of current, i_{sq} varied and matched with reference i^*_{sq} for speed and load torque variations but remained immune to stator resistance variation (as in Fig. 4f). In practice, stator resistance will not vary so much and never in step. Such a high step is considered here to show the effectiveness of the proposed algorithm. The output of the second order SMC current controllers, v^*_{sd} and v^*_{sq} are continuous signals as shown in Fig. 4e and the rotor flux orientation is maintained throughout as shown in Fig. 4g. This shows that chattering is eliminated with the use of second order sliding mode current controllers and at the same time decoupling is maintained between torque and flux for speed, load, or stator resistance parameter variations and thus the disturbances (as discussed in Section-IV) are rejected satisfactorily.

B. IM drive with second order SMC Current Controller at High Sampling Rate

As observed from (27), the dynamic response of u i.e., $\dot{u}$ can be increased with increasing sliding gains but very high sliding gains might introduce chattering even with second order controller. To overcome this problem and simultaneously achieve high dynamic response, higher sliding gains can be employed at higher sampling rates (or lower sampling time period). This can be understood from (30) where it can be observed that the product of sampling time period (T_s) and sliding gains contribute to u_k. Therefore, by decreasing T_s, we can have higher sliding gains keeping their product constant effectively increasing the dynamic response without introducing chattering. This is demonstrated in simulation using Fig. 5 where the sampling frequency ($F_s = 1/T_s$) is 195.312 kHz. Similar reference commands are given here also as shown in Fig. 5 except that the second order controller gains are now increased as shown in Table II. Disturbance rejection is achieved here also as observed from d- and q-axis stator current waveforms presented in Fig. 5b and Fig. 5c. Along with this, dynamic response of q-axis current is now improved to around 2.5 ms as shown in Fig. 5d without disturbing d-axis current shown in Fig. 5b. Chattering free stator voltages in d-q frame are shown in Fig. 5e and the stator resistance variation done is shown in Fig. 5f. The flux orientation is well maintained as shown in Fig. 5g. Therefore, similarly the dynamic response can be further improved at much higher sampling rates simutaneously maintaining disturbance rejection.

C. IM drive with second order SMC Current Controller at High Sampling Rate with R_r variation

As discussed in Section IV-C, the rotor time constant disturbances cannot be rejected in indirect vector controlled induction motor drive. Though it is not possible to access the rotor winding to experiment in a squirrel cage induction motor, it is possible to verify this in simulation which uses the mathematical model of the machine. This is demonstrated in Fig. 6 where rotor time constant is varied by varying rotor resistance R_r as shown in Fig. 6e. It can be observed from Figs. 6b and 6c that both d- and q-axis currents are matching their reference values at all times. Therefore, the sliding controllers are working fine but as seen from the d-q axis flux waveforms presented in Fig. 6f, the rotor flux orientation is completely lost when R_r is varied from its nominal value. This is because the actual sensed currents are transformed to d-q frame using rotor time constant dependent

transformation and fed to the sliding controller which blindly matches the reference with actual and hence this disturbance cannot be rejected. The reference voltages are shown in Fig. 6d and the speed response can be observed from Fig. 6a where the actual speed also varied with R_r disturbance. The results are in coherence with the explanation presented in Section IV-C.

VIII. Experimental Set-up

A. Prototype Description

A laboratory prototype is developed to validate the proposed scheme. A Xilinx based FPGA (SPARTAN XC3S1400an) controller board is used for this purpose. The photographic view of the hardware set-up is shown in Fig. 9. The FPGA board consists of logic gates, external ADC (ADS8361) and DAC (DAC8554) and dedicated I/O ports. The PWM pulses generated from FPGA board are fed to the gate driver of the IGBT inverter through an op-amp circuit that shifts the voltage level of 3.3V (from FPGA) to 15V. The motor currents are sensed through current sensors (LA-55P) and given to the controller board (FPGA) with the help of ADC. Speed of the motor is obtained from the speed encoder. The encoder pulses are given to the I/O pins of FPGA board via a buffer circuit. The induction machine (details in Table I) is coupled with a separately excited dc machine. For loading the induction machine, the dc machine armature is current controlled through a four quadrant dc chopper.

IX. Experimental Results

Experimental results are obtained from a laboratory developed prototype, as discussed in Section-VIII. The FPGA resource utilization for implementing the entire algorithm is found to be about 25% and hence this algorithm can be easily implemented in much cheaper FPGAs. It must be noted that the code complexity remains same whatever the sampling frequency since it is parallel implementation and the highest sampling rate is only limited by the ADC sampling rate and the FPGA clock whichever is lower. In this case, the ADC conversion rate was lower and approximately equal to 250 kHz. All the results are observed through DACs interfaced with the FPGA board. In the waveforms presented, 1V correspond to 10rad/s of speed, 1.018Wb of flux, 80V of voltage, and 1.697A of current. Similar loading and stator resistance parameter variation conditions are maintained as detailed in simulation and the machine parameters are the same as given in Table I.

A. IM drive with second order SMC Current Controller

The experimental result for the second order SMC current controller fed IM drive corresponding to the simulation in Fig. 4 is shown in Fig. 7. The switching frequency of the inverter and sampling frequency of the system are chosen to be same and equal to be 6.103 kHz (same value as in simulation). The reference and actual speeds are matching as shown in Fig. 7a. Chattering free decoupled i_{sd} and i_{sq} waveforms are shown in Figs. 7b and 7c respectively where they match their corresponding simulation results. The magnified response of i_{sq} current dynamics is shown in Fig. 7d. Rotor flux (as seen

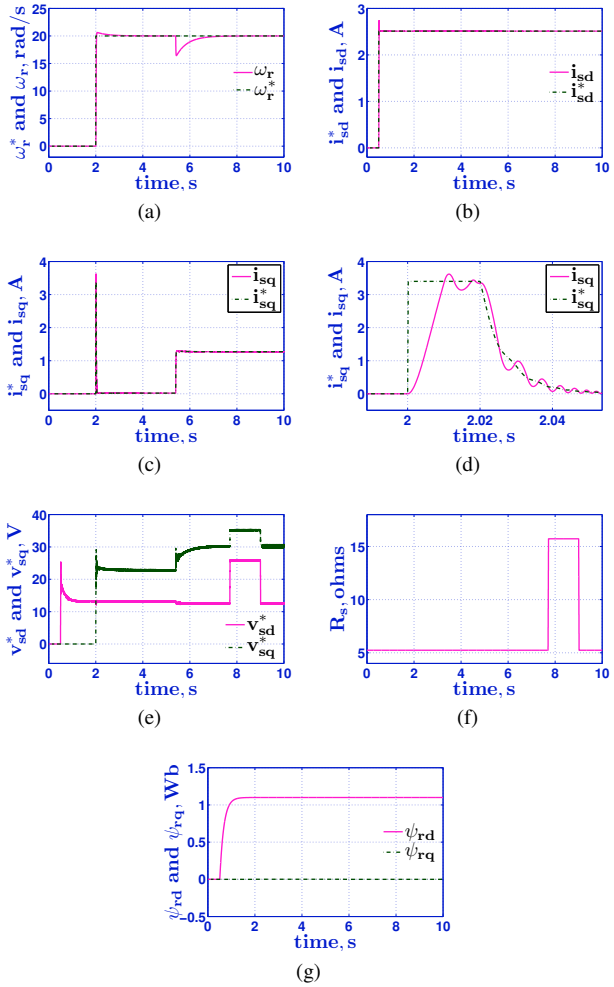

Fig. 4. Simulation result for second order SMC current controller fed IM drive. (a) ω_r^* and ω_r vs. time. (b) i_{sd}^* and i_{sd} vs. time. (c) i_{sq}^* and i_{sq} vs. time. (d) i_{sq}^* and i_{sq} vs. time. (e) v_{sd}^* and v_{sq}^* vs. time. (f) R_s vs. time. (g) ψ_{rd} and ψ_{rq} vs. time.

from i_{sd} waveform in Fig. 7b and from d-q flux waveforms in Fig. 7f) is well oriented irrespective of speed, load, or stator resistance parameter variation (Fig. 4f). The outputs of the second order SMC, v_{sd}^* and v_{sq}^* are shown in Fig. 7e. It can be observed from Fig. 7e that v_{sd}^* and v_{sq}^* vary almost instantaneously for speed, load, and stator resistance parameter variation thus maintaining decoupling between i_{sd} and i_{sq} waveforms. This proves the superiority of using second order SMC current controllers over hysteresis current controllers because the switching frequency is constant and decoupling is inherently maintained by rejecting disturbances.

B. IM drive with second order SMC Current Controller at High Sampling Rate

The experimental result corresponding to the higher sampling rate implementation of the same algorithm is shown in Fig. 8. While the sampling rate is increased to 195.312 kHz (same as in simulation), the switching frequency of the inverter is kept constant at 6.103 kHz itself. Therefore, only difference is in the algorithm implementation in FPGA

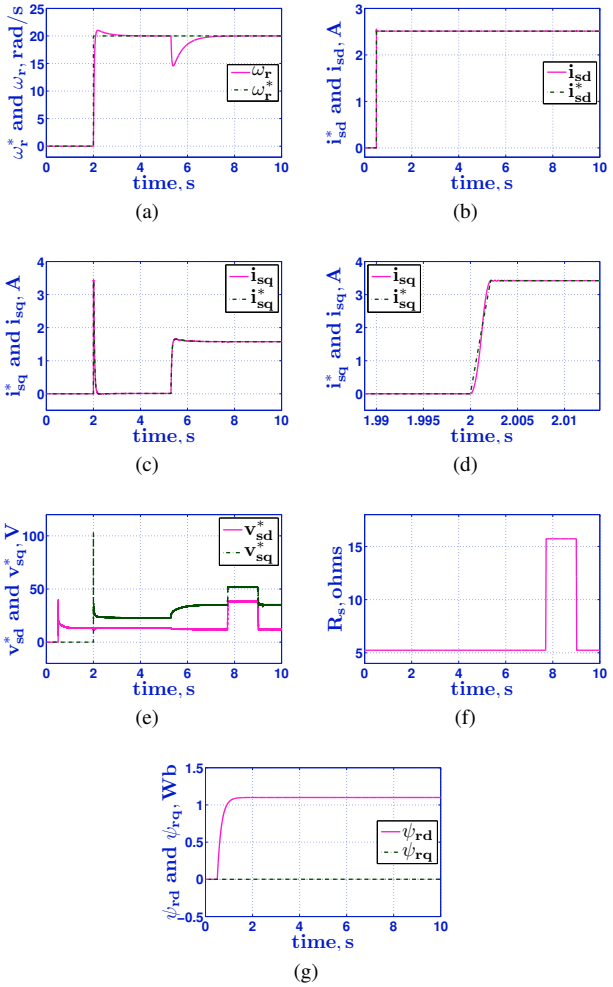

Fig. 5. Simulation result for second order SMC Current Controller at High Sampling Rate. (a) ω_r^* and ω_r vs. time. (b) i_{sd}^* and i_{sd} vs. time. (c) i_{sq}^* and i_{sq} vs. time. (d) i_{sq}^* and i_{sq} vs. time. (e) v_{sd}^* and v_{sq}^* vs. time. (f) R_s vs. time. (g) ψ_{rd} and ψ_{rq} vs. time.

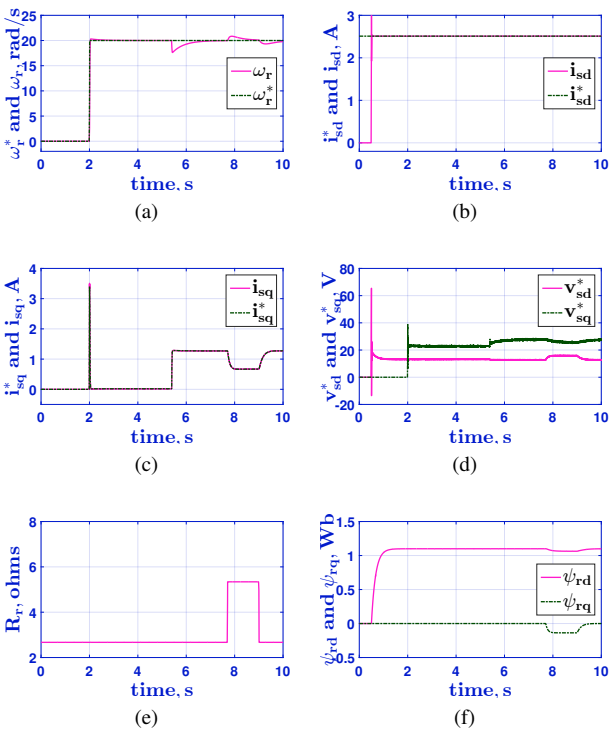

Fig. 6. Simulation result for second order SMC Current Controller at High Sampling Rate with R_r variation. (a) ω_r^* and ω_r vs. time. (b) i_{sd}^* and i_{sd} vs. time. (c) i_{sq}^* and i_{sq} vs. time. (d) i_{sq}^* and i_{sq} vs. time. (e) v_{sd}^* and v_{sq}^* vs. time. (f) R_s vs. time. (g) ψ_{rd} and ψ_{rq} vs. time.

and there is absolutely no change in the power circuit i.e, the inverter and machine operation. FPGA, being a parallel processor is the best candidate for such implementation and the controller gains are as shown in Table II. Similar conditions are maintained as in the corresponding simulation result (Fig. 5) where the drive is tested for both matched and un-matched disturbances. The d-axis stator current (reference and actual) are shown in Fig. 8b where the actual tracks the reference and stays there irrespective of disturbances (load torque and R_s variation). The i_{sq} reference and actual waveforms are shown in Fig. 8c where it rejects R_s variation disturbance (Fig. 5f). The dynamic response of torque (i_{sq})is now improved to 2.5 ms as shown in Fig. 8d. Thus, the d- and q-axes maintain decoupling between each other while rejecting disturbances and this can be reaffirmed from the d- and q-flux waveforms shown in Fig. 8f. All these advantages combine with high dynamic response at higher sampling rates as shown. Sampling rates higher than 195.312 kHz as shown could not be achieved due to ADC limitation otherwise much faster dynamic response is practically possible.

TABLE I
INDUCTION MACHINE RATING AND PARAMETERS

Parameter	Symbol	Nominal Value
Rated Shaft Power	-	1.3 kW
Line to Line Voltage	-	400 V
Phase Current	-	3 A
Rated Speed	-	1430 rpm
Number of Poles	p	4
Stator Self-Inductance	L_s	0.4525 H/ph
Rotor Self-Inductance	L_r	0.4525 H/ph
Magnetizing Inductance	L_m	0.4381 H/ph
Stator Resistance	R_s	5.24 Ω/ph
Rotor Resistance	R_r	2.67 Ω/ph
Machine Inertia	J	0.011 kg-m^2
Viscous Coefficient	B	0.0015

X. CONCLUSION

This paper has investigated in deep details the important issues of sliding mode control and presented the disturbance rejection ability of such controller (first or second order) in vector controlled induction motor drive. It is shown that the drive can reject matched (parameter variations) as well as unmatched disturbances (load torque variations) as long as the conditions for disturbance rejection are satisfied. Also, it is shown that there are disturbances that cannot be rejected for such systems. This is due to the fact that the sensed signals (currents) are not directly fed into the sliding controller.

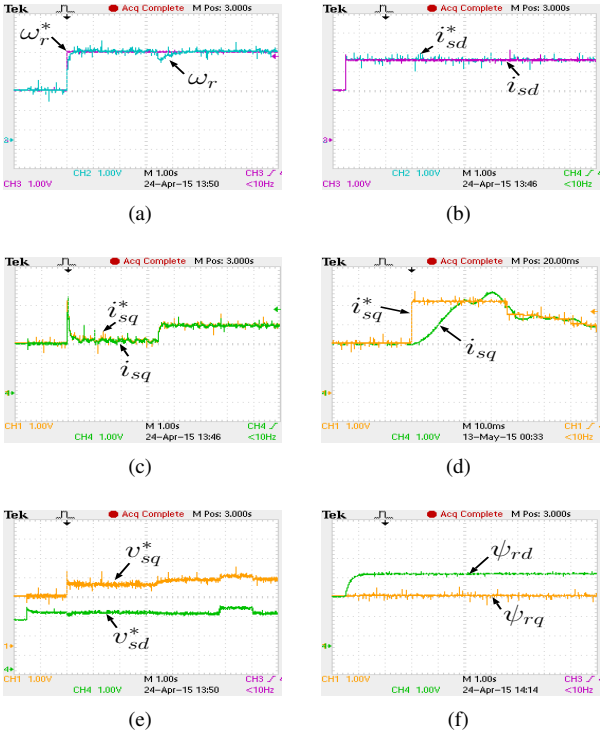

Fig. 7. Experimental result for second order SMC current controller fed IM drive. (a) ω_r^* and ω_r vs. time. (b) i_{sd}^* and i_{sd} vs. time. (c) i_{sq}^* and i_{sq} vs. time. (d) i_{sq}^* and i_{sq} vs. time. (e) v_{sd}^* and v_{sq}^* vs. time. (f) ψ_{rd} and ψ_{rq} vs. time.

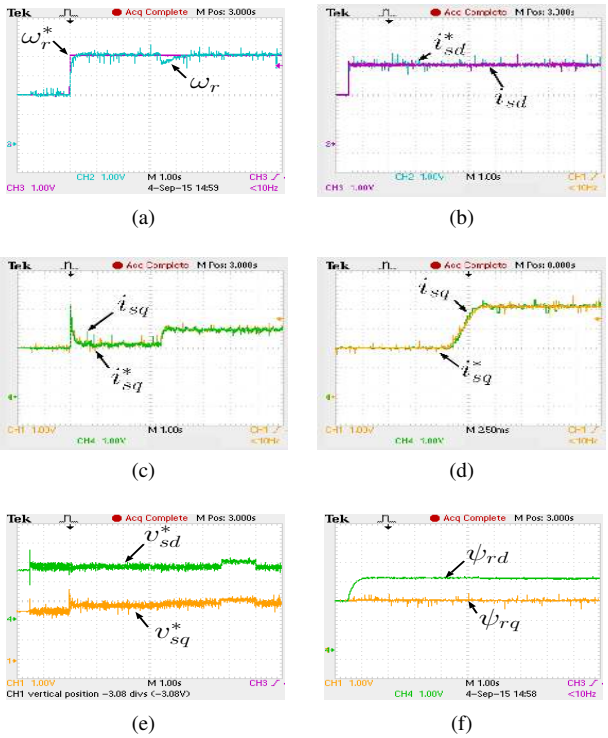

Fig. 8. Experimental result for second order SMC current controller fed IM drive at High Sampling Rate. (a) ω_r^* and ω_r vs. time. (b) i_{sd}^* and i_{sd} vs. time. (c) i_{sq}^* and i_{sq} vs. time. (d) i_{sq}^* and i_{sq} vs. time. (e) v_{sd}^* and v_{sq}^* vs. time. (f) ψ_{rd} and ψ_{rq} vs. time.

TABLE II
CONTROLLER VALUES

Symbol	Parameter	$F_s =$ 6.103 kHz	$F_s =$ 195.3 kHz
k_{p1}, k_{i1}	Speed PI Controller	0.25, 0.52	0.25, 0.52
r_{12}, r_{22}	d-controller (SMC)	2400, 80	51200, 1280
r_{11}, r_{21}	q-controller (SMC)	1800, 100	25200, 1400

MATLAB/Simulink based simulations and experimental verifications confirmed the usefulness of the proposed system. Issues related to development of low cost controller using FPGA are presented. Improvement in dynamic response using higher sampling rate is experimentally demonstrated.

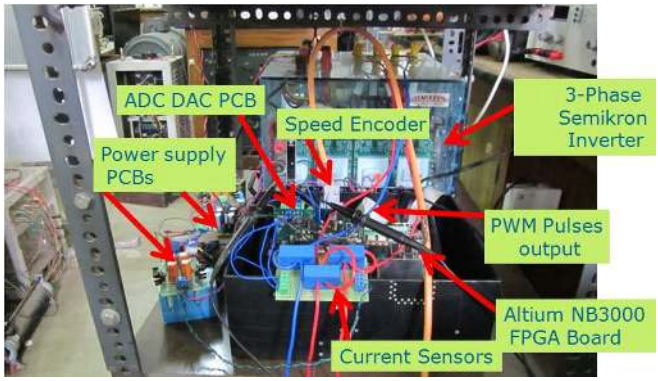

Fig. 9. View of the experimental setup.

REFERENCES

[1] V. I. Utkin, *Sliding Modes and their Application in Variable Structure Systems*, 1st ed. Moscow: MIR, 1978.

[2] L. Zhao, J. Huang, H. Liu, B. Li, and W. Kong, "Second-Order Sliding-Mode Observer With Online Parameter Identification for Sensorless Induction Motor Drives," *IEEE Trans. Ind. Electron.*, vol. 61, no. 10, pp. 5280–5289, Oct. 2014.

[3] M. Comanescu, "Design and Implementation of a Highly Robust Sensorless Sliding Mode Observer for the Flux Magnitude of the Induction Motor," *IEEE Trans. Energy Convers.*, vol. 31, no. 2, pp. 649–657, Jun. 2016.

[4] R. Padilha Vieira, C. Cauduro Gastaldini, R. Zelir Azzolin, and H. Grundling, "Sensorless Sliding-Mode Rotor Speed Observer of Induction Machines Based on Magnetizing Current Estimation," *IEEE Trans. Ind. Electron.*, vol. 61, no. 9, pp. 4573–4582, Sep. 2014.

[5] S. Hasan and I. Husain, "A Luenberger Sliding Mode Observer for Online Parameter Estimation and Adaptation in High-Performance Induction Motor Drives," *IEEE Trans. Ind. Appl.*, vol. 45, no. 2, pp. 772–781, Mar. 2009.

[6] C. Lascu, I. Boldea, and F. Blaabjerg, "A Class of Speed-Sensorless Sliding-Mode Observers for High-Performance Induction Motor Drives," *IEEE Trans. Ind. Electron.*, vol. 56, no. 9, pp. 3394–3403, Sep. 2009.

[7] A. Saghafinia, H. W. Ping, M. Uddin, and K. Gaeid, "Adaptive Fuzzy Sliding-Mode Control Into Chattering-Free IM Drive," *IEEE Trans. Ind. Appl.*, vol. 51, no. 1, pp. 692–701, Jan. 2015.

[8] W. C. A. Pereira, C. M. R. Oliveira, M. P. Santana, T. E. P. Almeida, A. G. Castro, G. T. Paula, and M. L. Aguiar, "Improved Sensorless Vector Control of Induction motor Using Sliding Mode Observer," *IEEE Latin America Transactions*, vol. 14, no. 7, pp. 3110–3116, Jul. 2016.

[9] S. Di Gennaro, J. Rivera Dominguez, and M. Meza, "Sensorless High

Order Sliding Mode Control of Induction Motors With Core Loss," *IEEE Trans. Ind. Electron.*, vol. 61, no. 6, pp. 2678–2689, Jun. 2014.
[10] G. Rubio-Astorga, J. D. Sánchez-Torres, J. Cañedo, and A. G. Loukianov, "High-Order Sliding Mode Block Control of Single-Phase Induction Motor," *IEEE Trans. Control Syst. Technol.*, vol. 22, no. 5, pp. 1828–1836, Sep. 2014.
[11] M. T. Angulo and R. V. Carrillo-Serrano, "Estimating rotor parameters in induction motors using high-order sliding mode algorithms," *IET Control Theory Appl.*, vol. 9, no. 4, pp. 573–578, 2015.
[12] K. Corzine, "A hysteresis current-regulated control for multi-level drives," *IEEE Trans. Energy Convers.*, vol. 15, no. 2, Jun. 2000.
[13] F. Wu, F. Feng, L. Luo, J. Duan, and L. Sun, "Sampling Period Online Adjusting-Based Hysteresis Current Control Without Band With Constant Switching Frequency," *IEEE Trans. Ind. Electron.*, vol. 62, no. 1, pp. 270–277, Jan. 2015.
[14] D. Traore, F. Plestan, A. Glumineau, and J. De Leon, "Sensorless Induction Motor: High-Order Sliding-Mode Controller and Adaptive Interconnected Observer," *IEEE Trans. Ind. Electron.*, vol. 55, no. 11, pp. 3818–3827, Nov. 2008.
[15] M. Rashed, K. B. Goh, M. W. Dunnigan, P. F. A. MacConnell, A. F. Stronach, and B. W. Williams, "Sensorless second-order sliding-mode speed control of a voltage-fed induction-motor drive using nonlinear state feedback," *IEE Proc. on Elect. Pow. Appl.*, vol. 152, no. 5, pp. 1127–1136, Sep. 2005.
[16] C. Lascu, S. Jafarzadeh, M. S. Fadali, and F. Blaabjerg, "Direct Torque Control With Feedback Linearization for Induction Motor Drives," *IEEE Trans. Power Electron.*, vol. 32, no. 3, pp. 2072–2080, Mar. 2017.
[17] A. Pisano, A. Davila, L. Fridman, and E. Usai, "Cascade Control of PM DC Drives Via Second-Order Sliding-Mode Technique," *IEEE Trans. Ind. Electron.*, vol. 55, no. 11, pp. 3846–3854, Nov. 2008.
[18] A. Levant, "Sliding order and sliding accuracy in sliding mode control," *International Journal of Control*, vol. 58, no. 6, pp. 1247–1263, 1993.
[19] G. Bartolini, A. Ferrara, and E. Usani, "Chattering avoidance by second-order sliding mode control," *IEEE Trans. Autom. Control*, vol. 43, no. 2, pp. 241–246, Feb. 1998.
[20] A. Levant, "Higher-order sliding modes, differentiation and output-feedback control," *International Journal of Control*, vol. 76, no. 9-10, pp. 924–941, 2003.
[21] M. Comanescu, L. Xu, and T. Batzel, "Decoupled Current Control of Sensorless Induction-Motor Drives by Integral Sliding Mode," *IEEE Trans. Ind. Electron.*, vol. 55, no. 11, pp. 3836–3845, Nov. 2008.
[22] J. Ye, P. Malysz, and A. Emadi, "A fixed-switching-frequency integral sliding mode current controller for switched reluctance motor drives," *IEEE Journal of Emerging and Selected Topics in Power Electronics*, vol. 3, no. 2, pp. 381–394, Jun. 2015.
[23] S. K. Kommuri, J. J. Rath, K. C. Veluvolu, M. Defoort, and Y. C. Soh, "Decoupled current control and sensor fault detection with second-order sliding mode for induction motor," *IET Control Theory Appl.*, vol. 9, no. 4, pp. 608–617, Feb. 2015.
[24] A. Estrada and L. Fridman, "Integral HOSM Semiglobal Controller for Finite-Time Exact Compensation of Unmatched Perturbations," *IEEE Trans. Autom. Control*, vol. 55, no. 11, pp. 2645–2649, Nov. 2010.
[25] A. V. Ravi Teja, C. Chakraborty, S. Maiti, and Y. Hori, "A New Model Reference Adaptive Controller for Four Quadrant Vector Controlled Induction Motor Drives," *IEEE Trans. Ind. Electron.*, vol. 59, no. 10, pp. 3757–3767, Oct. 2012.
[26] A. Levant, "Quasi-continuous high-order sliding-mode controllers," *IEEE Trans. Autom. Control*, vol. 50, no. 11, pp. 1812–1816, Nov. 2005.
[27] H. Oza, Y. Orlov, and S. Spurgeon, "Tuning rules for second order sliding mode based output feedback synthesis," in *Proc. of the 12th International Workshop on Variable Structure Systems, VSS 2012*, Jan. 2012, pp. 130–135.

A. V. Ravi Teja (M'17) received the B.E. degree in Electrical and Electronics Engineering from Osmania University, Hyderabad, India in 2008, the M. Tech. and Ph.D. degree in Electrical Engineering from Indian Institute of Technology Kharagpur, Kharagpur, India in 2010 and 2016, respectively. He is currently working as an Assistant Professor in the Department of Electrical Engineering at IIT Ropar, India. His research areas of interest include electric machine drives, power electronics, and control systems.

Chandan Chakraborty (S'92-M'97-SM'01-F'15) received the B.E. and M.E. degrees in electrical engineering from Jadavpur University, Kolkata, India, in 1987 and 1989, respectively,and Ph.D. degrees from the Indian Institute of Technology Kharagpur, Kharagpur, India, and Mie University, Tsu, Japan, in 1997 and 2000, respectively. He is a Professor with the Department of Electrical Engineering, Indian Institute of Technology Kharagpur, Kharagpur, India. His research interests include power converters, motor drives, electric vehicles, and renewable energy. Dr. Chakraborty was awarded the Japan Society for the Promotion of Science Fellowship to work at The University of Tokyo, Tokyo, Japan, during 2000–2002. He received the Bimal Bose Award in power electronics from the Institution of Electronics and Telecommunication Engineers (India) in 2006. He is an Administrative Committee Member of the IEEE Industrial Electronics Society. He is one of the Editors of the IEEE TRANSACTIONS ON SUSTAINABLE ENERGY and IEEE Power Engineering Letters and an Associate Editor of IEEE TRANSACTIONS ON INDUSTRIAL ELECTRONICS and the IEEE Industrial Electronics Magazine. He is a Fellow of the Indian National Academy of Engineering.

Bikash C. Pal (M'00-SM'02-F'13) received B.E.E. (with honors) degree from Jadavpur University, Calcutta, India, M.E. degree from the Indian Institute of Science, Bangalore, India, and Ph.D. degree from Imperial College London, London, U.K., in 1990, 1992, and 1999, respectively, all in electrical engineering. Currently, he is a Professor in the Department of Electrical and Electronic Engineering, Imperial College London. He was Editor-in-Chief of IEEE Transactions on Sustainable Energy (2012-2017) and Editor-in-Chief of IET Generation, Transmission and Distribution (2005-2012) and is a Fellow of IEEE for his contribution to power system stability and control. His current research interests include renewable energy modelling and control, state estimation, and power system dynamics.